



 Cite this: *CrystEngComm*, 2017, 19, 5686

# Pd–Au heterostructured nanonecklaces with adjustable interval and size as a superior catalyst for degradation of 4-nitrophenol†

 Zhao Huang,<sup>‡</sup> Kai Cai,<sup>‡</sup> Huan Zhang, Zilan Hong, Zhaodong Yuan and Heyou Han \*

A facile method for the synthesis of Au-pearl/Pd-wire heterostructured nanonecklaces (APHNs) was developed for the first time, in which regular Au pearls with controllable size and interval distance were interlinked into a string by an ultrathin and ultralong Pd nanowire. The distribution density of Au nanoparticles was regulated by the concentration of the reducing agent, while their size was controlled by the amount of the Au precursor. In the study of degradation of 4-nitrophenol (4-NP), the catalytic properties of several typical APHNs are proved to be inherently related to their morphology. By comparison with other nanostructures and commercial Pd/C, the APHNs show superior catalytic activities and better stability in general. The study demonstrated that novel heterostructures have superior catalytic properties in the degradation of 4-NP. Moreover, the nanostructures have the potential to be used as a high-efficiency catalyst in other catalytic reactions.

 Received 24th June 2017,  
Accepted 27th August 2017

DOI: 10.1039/c7ce01174a

[rsc.li/crystengcomm](http://rsc.li/crystengcomm)

## Introduction

Palladium (Pd) is used as a main catalyst in many reactions for industrial and commercial purposes, especially in organic reactions.<sup>1</sup> Pd-based bimetallic nanostructures, including alloy, core–shell and heterostructured nanomaterials, have received great attention due to their enhanced properties compared with the monometallic Pd counterparts in various catalytic reactions.<sup>2–9</sup> Among them, PdAu bimetallic materials show good prospects due to the combined effects of Pd and Au, which reduce the binding strength between Pd and reactants and improve the poisoning-resistance of Pd.<sup>9–13</sup>

Heteronanostructures are widely recognized for their good performances and great potential in various applications, because they may possess new functions due to a synergistic effect besides the intrinsic properties of the two distinct metals.<sup>14–17</sup> However, due to their different parameters, such as shape, size and relative locations of different components, they have highly diverse physical and chemical properties.<sup>18–20</sup> Particularly, in a structure, the same element

in different positions could induce distinct reaction pathways towards the same reactant.<sup>21</sup> Therefore, it is very significant to design PdAu heterostructures with a controlled morphology for more desirable properties.

In recent years, a few PdAu heterostructures have been reported and certain progress has been achieved.<sup>9,22,23</sup> For example, the interface of Pd and Au on heterostructured nanotubes was demonstrated to play a vital role in their enhanced electrocatalytic activity.<sup>23</sup> Very recently, our group reported Au-island-covered Pd nanotubes and studied the catalytic properties of the nanotubes with different ratios of Au in the electrooxidation of alcohol. The optimized structures exhibited an outstanding catalytic activity.<sup>9</sup> However, the studies of PdAu heterostructures are still very limited so far, especially the studies of the relationships between the catalytic properties and physical parameters, because they require precise regulation of the shape, size and location of the different components of the heterostructures.<sup>23,24</sup>

According to previously published studies, in the synthesis of Au-containing heterostructures, including dimer or polymer hybrid nanoparticles, core/satellite configuration and so on, a unit is usually obtained at first, which is then used as the seed or main component for further growth or selective deposition of other units.<sup>25–30</sup> Hence, the process of synthesizing heterostructures is generally more intricate than the synthesis of corresponding alloy and core–shell structures. Based on the above analyses, to develop a simple and reliable method for controllable synthesis of PdAu heterostructures is highly desirable.

State Key Laboratory of Agricultural Microbiology, College of Science, Huazhong Agricultural University, Wuhan 430070, China. E-mail: [hyhan@hzau.edu.cn](mailto:hyhan@hzau.edu.cn)

† Electronic supplementary information (ESI) available: TEM images of Te NWs, Pd nanowires, and Au nanoparticles. EDS, XRD, UV-vis spectra and XPS of Pd–Au heterostructured nanonecklaces. TEM images of Pd–Au heterostructured nanonecklaces synthesized using different amounts of AA. Plots of  $C_t/C_0$  and  $\ln(C_t/C_0)$  versus reaction time for the reduction of 4-NP over APHNs and the mixture of Pd nanowires and Au nanoparticles. See DOI: 10.1039/c7ce01174a

‡ Zhao Huang and Kai Cai contributed equally to this work.

In this work, we first demonstrated the synthesis of a novel type of structure, Au-pearl/Pd-wire heterostructured nanonecklaces (APHNs), in which ultrathin and ultralong Pd nanowires interlink many regular Au nanoparticles into a string. The interval of adjacent Au nanoparticles could be simply regulated by the concentration of the reducing agent, and the size of the nanoparticles could be controlled by the amount of the Au precursor. It is worth noting that this work is very different from our previous research.<sup>9,31</sup> Firstly, in this work, ultrathin and ultralong Te nanowires were used, which enable the precise adjustment and clear characterization of the nanostructures. Furthermore, the adjustment of the interval of Au nanoparticles depended on the supply of the reducing agent. The novel nanostructures were used in the catalytic reduction of 4-nitrophenol (4-NP) by NaBH<sub>4</sub>, and they exhibited a structure-related catalytic activity. Compared with commercial Pd/C and the physical mixture of Pd nanowires and Au nanoparticles, the optimized APHNs exhibited an outstanding catalytic activity and durability.

## Experimental section

### Reagents and materials

Hydrazine monohydrate (85%, AR), acetone (99%, AR), ethanol (99.7%, AR), tetrachloroauric(III) acid hydrate (HAuCl<sub>4</sub>·4H<sub>2</sub>O, AR), palladium(II) chloride (PdCl<sub>2</sub>, AR), polyvinyl pyrrolidone (PVP), sodium borohydride (NaBH<sub>4</sub>), ascorbic acid (AA, AR), ammonium hydroxide (25%, AR), hydrochloric acid (HCl, AR) and sodium tellurite (Na<sub>2</sub>TeO<sub>3</sub>, 99.99%) were supplied by Sinopharm Chemical Reagent Co., Ltd. Hexadecyltrimethylammonium bromide (CTAB, 99%) was purchased from Sigma-Aldrich. 4-Nitrophenol (4-NP) was commercially available from Aladdin Chemistry Co., Ltd. The commercial Pd/C catalyst (20 wt%) was purchased from BASF.

### Characterization

Transmission electron microscopy (TEM) measurements were carried out using a JEM-2100F high-resolution transmission electron microscope at an accelerating voltage of 200 kV. Scanning transmission electron microscopy (STEM) elemental maps were obtained under the high-angle annular dark field (HAADF) mode using a FEI TECNAIF-30 microscope operated at 300 kV. X-ray diffraction (XRD) measurement was carried out on a Bruker D8 Advance X-ray diffractometer with Cu K $\alpha$  radiation. Ultraviolet-visible (UV-vis) absorption spectra were recorded on a Perkin-Elmer Lambda 25 UV-vis spectrometer. Inductively coupled plasma atom emission spectroscopy (ICP-AES) measurements used an IRIS Intrepid II XSP instrument (Thermo Fisher Scientific, USA). X-ray photoelectron spectroscopy (XPS) measurements used a Thermo Fisher ESCALAB 250Xi spectrophotometer with an AlK $\alpha$  radiator.

### Synthesis of ultrathin and ultralong Te nanowires

The ultrathin and ultralong Te NWs were prepared according to a previous method. Typically, Na<sub>2</sub>TeO<sub>3</sub> (0.072 g), PVP (0.80

g) and H<sub>2</sub>O (25 mL) were added to a beaker. After the dissolution of Na<sub>2</sub>TeO<sub>3</sub> under magnetic stirring at room temperature, the solution was transferred into a Teflon bottle containing ammonium hydroxide (2.67 mL) and hydrazine monohydrate (1.35 mL). The bottle was maintained in an autoclave at 180 °C for 3.5 h. After cooling down, the as-prepared materials in the solution were precipitated with acetone (88 mL), then were centrifuged (10 000 rpm, 15 min) and washed several times with ethanol and ultrapure water. The as-prepared materials were dispersed in H<sub>2</sub>O (15 mL).

### Synthesis of Au-pearl/Pd-wire heterostructured nanonecklaces

In a typical synthesis, Te NWs (0.10 mL) from the previous experiment were dispersed in 6 mL of CTAB solution (4.55 mg mL<sup>-1</sup>, distilled water as solvent) under constant magnetic stirring at 40 °C. After 10 min, PdCl<sub>2</sub> solution (5 mM, 200  $\mu$ L) was added to the solvent with the color changed from blue to grey-black. After another 15 min, AA (40 mM, 350  $\mu$ L) was added and stirred for 10 min before HAuCl<sub>4</sub> (5 mM, 200  $\mu$ L) was added to the solution. The mixture was subjected to a centrifugation/wash (7000 rpm, 7 min) cycle to remove most of the matrices after 20 min. In the synthesis, experimental parameters are the same as those mentioned above unless specifically stated.

### Synthesis of Au nanoparticles and Pd nanowires

In a typical synthesis, Te NWs (0.10 mL) from the previous experiment were dispersed in 6 mL of CTAB solution (4.55 mg mL<sup>-1</sup>) under constant magnetic stirring at 40 °C. After 10 min, HAuCl<sub>4</sub> (5 mM, 80  $\mu$ L) was added to the solution. 50 min later, the product was obtained after being centrifuged (7000 rpm, 7 min) and washed. In the synthesis of Pd nanowires, PdCl<sub>2</sub> (5 mM, 250  $\mu$ L) was added to replace HAuCl<sub>4</sub> and then AA (30 mM, 350  $\mu$ L) was added.

### Catalytic degradation of 4-nitrophenol (4-NP)

Typically, 2.0 mL of ultrapure water, 100  $\mu$ L of 4-NP solution (1.0 mM) and 0.2 mL of freshly prepared NaBH<sub>4</sub> aqueous solution (0.1 M) were added to a standard quartz cuvette at room temperature. Subsequently, APNTs (10.25  $\mu$ g) were added to the solution. Changes in the concentration of 4-NP were monitored by UV-vis absorption in the scanning range of 250–550 nm.

For the durability test, 50  $\mu$ L of 4-NP solution (1.0 mM) and 100  $\mu$ L of NaBH<sub>4</sub> aqueous solution (0.1 M) were added in sequence into the quartz cuvette after the first measurement and UV-vis spectroscopy was used to record the absorption in the course of time. The test was repeated seven times in the same reaction system. The qualities of Pd or Au in all APHNs and the control group are identical in the measurement.

## Results and discussion

The ultrathin and ultralong Te nanowires were firstly synthesized through a hydrothermal process according to a

previously reported method.<sup>32</sup> The transmission electron microscopy (TEM) images are shown in Fig. S1.† Their diameters are about 9 nm and the length is as long as 4–9  $\mu\text{m}$ .

Pd nanowires were obtained by galvanic replacement reaction using Te nanowires as the sacrifice template. Then Au nanopearls were heteroepitaxially grown on Pd nanowires. A typical TEM image of APHNs is shown in Fig. 1A. The magnified TEM image in Fig. 1B shows that many nanoparticles with similar sizes and interval distances are linked to a single nanowire which has the same diameter to the ultrathin Te nanowire template. The high-resolution TEM (HRTEM) image (Fig. 1C) of the structure shows that the adjacent lattice fringes of the nanowire segment and the pearl are 0.22 and 0.24 nm, which correspond to the lattice spacing of the (111) planes of face-centered-cubic (fcc) Pd and Au, respectively. High-angle annular dark-field (HAADF) scanning transmission electron microscopy (STEM) was used in the element analysis. Fig. 1D shows the elemental mapping of a part of the material. It is clearly shown that the middle nanowire segment is composed of Pd and the pearl is constituted by Au. The energy-dispersive X-ray spectrum (EDS) (Fig. S2†) shows that the APHNs are primarily composed of Au and Pd. Moreover, the X-ray diffraction (XRD) patterns of the structures (Fig. S3†) show that all peaks match the fcc phase of Au and Pd. Fig. S4† shows the absorption spectra of the nanostructures. The visible peak at about 520 nm is attributed to the Au nanopearls. Moreover, X-ray photoelectron spectroscopy (XPS) was used to analyze the near-surface composition of the structures. The Au 4f and Pd 3d spectra are shown in Fig. S5.† The doublets at 84.0 and 87.7 eV are the signatures of zero valent Au, and the doublets at 341.0 and 335.8 eV are the signatures of zero valent Pd. The above results demonstrate that the products are heterostructured nanonecklaces consisting of Au nanopearls and Pd wires.

In the preparation, the interval distance and size of the Au nanopearls can be directly regulated by the amount of the reduc-

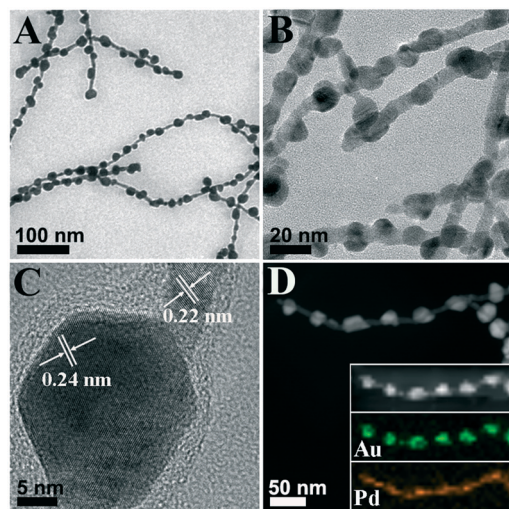


Fig. 1 TEM images (A and B) and HRTEM image (C) of APHNs. (D) EDS elemental mapping of Au and Pd in APHNs.

ing agent. To better illustrate the controllable strategy, a single variable was used for the synthesis of APHNs in three independent experiments, and the TEM images of the obtained APHNs are shown in Fig. 2. The amounts of the reducing agent and Au precursor are the variables in the horizontal and vertical column, respectively. That is, within the same experimental group (a, b, and c), the three experiments used the same Au precursor. The inset of Fig. 2 exhibits the statistical data of the interval distance and diameter of the nanopearls. It is shown that the interval distance of the nanopearls decreases with increasing amount of the reducing agent when the amount of the Au precursor is constant. At the same time, the size of the nanopearls becomes smaller with the increase in the total number of Au nanopearls. On the contrary, when the amount of the reducing agent is decreased, the interval distance and size of the nanopearls are increased.

A wide range of reducing agent concentrations (20–140 mM) were used to further study the regulation of the synthesis with fixed amount of the Au precursor. The TEM images are shown in Fig. S6.†

The statistical data of the size and interval distance of the nanopearls are listed in Fig. 3. The size and interval distance of the nanopearls consistently decrease with increasing amount of the reducing agent as a whole, and large variations could be observed at relatively lower concentrations. In addition, we used an extremely low concentration (5 mM) of the reducing agent in the synthesis, and the Au precursor was injected twice to validate the above findings. The results (Fig. S7A†) show that the Au nanopearls are widely scattered irregularly on

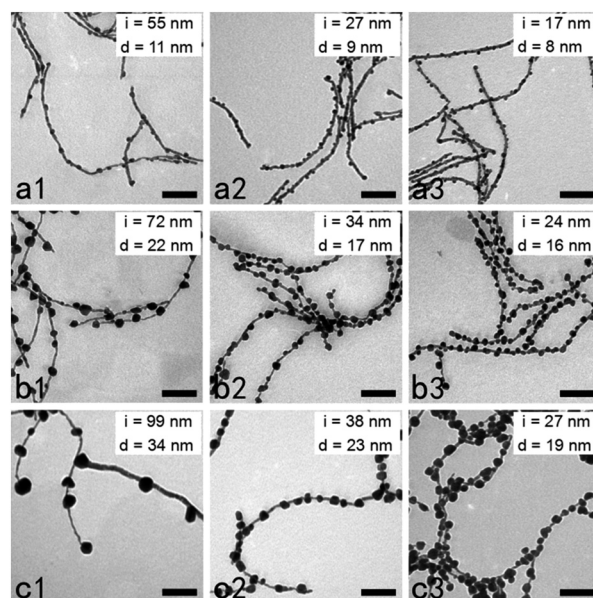


Fig. 2 TEM images of APHNs synthesized with different amounts of the reducing agent and Au precursor. (1), (2) and (3): 20, 100, and 200 mM ascorbic acid, respectively; (a), (b) and (c): 1.0, 5.0 and 10.0 mM  $\text{AuCl}_4^-$ , respectively. The volume of ascorbic acid,  $\text{AuCl}_4^-$ , Te nanowires and  $\text{PdCl}_2$  is 0.5, 0.5, 0.15 and 0.3 mL, respectively.  $i$  and  $d$  indicate interval and diameter, respectively. The values are the averages of 100 measurements.

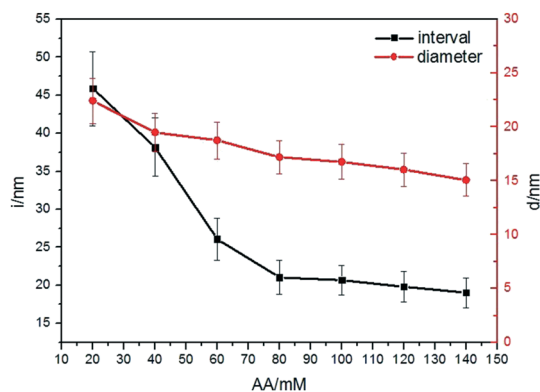


Fig. 3 The values of the interval and diameter of Au nanopearls. The values are the averages of 100 measurements.

the surface of the Pd nanowires after the first injection of the Au precursor. After the second injection, the size of the Au pearls increases and the interval distance shows no obvious change (Fig. S7B<sup>†</sup>). These observations are in complete conformity with the above conclusion that the concentration of the reducing agent can regulate the interval distance, and the amount of the Au precursor can adjust the size of the Au pearls in the method.

In the growth of bimetallic nanocrystals, many factors may affect the heterogeneous nucleation and growth, such as the lattice match, surface energy and surfactant.<sup>14</sup> Lattice mismatch (about 5%) naturally exists in Pd–Au bimetallic nanocrystals.<sup>24</sup> However, other physical parameters are changeable. For example, by using different reducing agents, PdAu core–shell or heterostructures could be obtained.<sup>23</sup> A typical synthesis can be divided into two distinct stages: 1) nucleation, 2) growth of seeds into nanocrystals.<sup>33</sup> In our synthesis, Pd nanowires are formed through a galvanic replacement reaction between the Pd precursor and Te nanowire templates. When the Au precursor is added into the solution containing the reducing agent, a great number of Au atoms are formed quickly. Pd nanowires provide numerous nucleation sites for the heterogeneous nucleation of Au atoms and thus Au nuclei are formed. In the second step, with the continuous supply of a large number of Au atoms, Au nuclei serve as seeds for further growth under suitable reaction conditions. Finally, Au pearls are formed on the surface of Pd nanowires. In the synthesis, a higher concentration of the reducing agent and Au precursor would lead to a more rapid formation of Au atoms, which greatly affects the formation of Au nuclei in the first step. Furthermore, the concentration of Au atoms directly affects the number of heterogeneous nuclei of Au pearls. Therefore, the concentration of the reducing agent affects the interval distance of the Au pearls.

Reduction of 4-nitrophenol (4-NP) to 4-aminophenol (4-AP) by NaBH<sub>4</sub> was employed as a model reaction to evaluate the catalytic activity of the APHNs. The conversion of 4-NP to 4-AP with reaction time was monitored by UV-vis spectrometry. As shown in Fig. 4, after injection of the catalyst into the solution containing 4-NP and NaBH<sub>4</sub>, the absorption peak at

400 nm, which is a characteristic peak of *p*-nitrophenolate ions, decreases in a time-dependent manner, and the peak at 300 nm which corresponds to *p*-aminophenol gradually increases. These variations would not occur when the solution does not contain a catalyst. A series of APHNs were prepared with different amounts of the reducing agent and were used as catalysts in the study, while the Pd/Au ratio was identical in all APHNs.

The reaction conversion is calculated from  $C_t/C_0$  at 400 nm, where  $C_t$  is the concentration at time  $t$  and  $C_0$  is the initial concentration. As the concentration of NaBH<sub>4</sub> is much higher than that of 4-NP, the reactions are assumed to be pseudo first-order with respect to the concentration of 4-NP. The linear correlation between  $\ln(C_t/C_0)$  and reaction time demonstrates that they are first-order reactions (Fig. 5A and Fig. S8A–G<sup>†</sup>). Therefore, the reaction rate constant  $k$ , an apparent first-order rate constant, can be used to evaluate the properties of the catalysts. The calculated results are shown in Fig. 5B. The value first rises to the highest and then declines. As the number of Pd–Au heterojunction interfaces increases with the increase of the concentration of the reducing agent added in the synthesis, the catalytic activity improves.<sup>9,22</sup> However, the exposed area of the Pd element decreases, which is caused by the coverage of Au nanopearls in the process. So, when the concentration of the reducing agent is excessively increased, the catalytic activity decreases on the whole, although the number of Pd–Au heterojunction interfaces increases. The highest value,  $8.1 \times 10^{-3} \text{ s}^{-1}$ , appears in the APHNs with an Au pearl size and interval distance of about 20 nm and 38 nm, respectively. For a quantitative study,  $k_{\text{Pd}}$ , a parameter defined as the ratio of rate constant  $k$  to the mass of Pd added, was introduced. According to the result of ICP-AES, the value of  $k_{\text{Pd}}$  is  $1670 \text{ s}^{-1} \text{ g}^{-1}$ , which is much higher than those of previously reported Pd-based nanostructures.<sup>34</sup>

The mixture of Pd nanowires and Au nanoparticles (Fig. S9<sup>†</sup>) was used for comparison in the study. The result (Fig. S8H<sup>†</sup>) shows that the catalytic activity of the contrast group is extremely low compared with APHNs. In addition, we also used the commercial Pd/C in the contrast experiment. The reaction rate constant was calculated to be  $4.8 \times 10^{-3} \text{ s}^{-1}$  ( $k_{\text{Pd}} = 990 \text{ s}^{-1} \text{ g}^{-1}$ ) (Fig. 5C). Furthermore, their reusabilities were

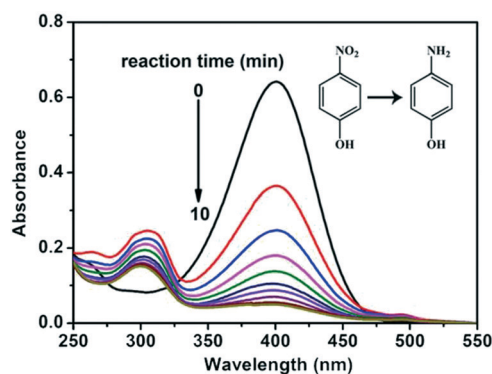
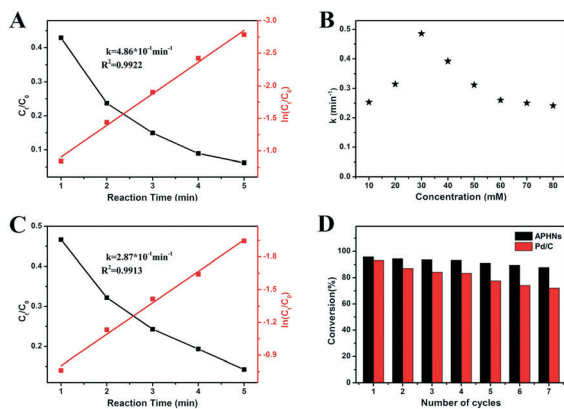


Fig. 4 Successive UV-vis absorption spectra of the reduction of 4-NP to 4-AP by NaBH<sub>4</sub> in the presence of APHNs.



**Fig. 5** Plots of  $C_t/C_0$  and  $\ln(C_t/C_0)$  versus reaction time for the reduction of 4-NP over APHNs (A) and commercial Pd/C (C). (B) Comparison of constant  $k$  values of APHNs catalysts obtained using different concentrations of AA (10, 20, 30, 40, 50, 60, 70 and 80 mM, 350  $\mu$ L) in HAuCl<sub>4</sub> (5 mM, 150  $\mu$ L). (D) Reusability of APHNs and the commercial Pd/C catalyst for the reduction of 4-NP with NaBH<sub>4</sub>.

evaluated by a stability test. As shown in Fig. 5D, after seven cycles, the conversions of the APHNs and Pd/C are 87.9% and 72.1%, respectively. The result demonstrates that the optimized heterostructures exhibit better catalytic activity and reusability than the commercial Pd/C. The superior properties of the Pd–Au catalyst are mainly attributed to their special structure. The abundant heterojunction interfaces probably provided high activity and the combination of Pd and Au improved the poisoning-resistance of Pd.<sup>13,22</sup>

## Conclusions

In summary, we have proposed a facile method to fabricate a novel type of Pd–Au heterostructure with the microscopic shape of a pearl necklace, in which ultrathin and ultralong Pd nanowires interlink many Au nanopearls into a string. Crucially, the size and interval distance of the adjacent Au nanopearls can be subtly regulated by the concentration of the Au precursor and reducing agent, respectively. Because the amount of the exposed Pd–Au interface is directly relevant to the density of the Au nanopearls, the heterostructured interface can be controlled by this method. In addition, the heterostructures exhibit superior catalytic properties, and display particular internal variation patterns with the density of the Au nanopearls. The novel Pd–Au heterostructures have the potential to be used as a catalyst for organic pollutant degradation, and the method provides a reliable route for the study of the relationship between the material structure and its catalytic properties.

## Conflicts of interest

There are no conflicts to declare.

## Acknowledgements

This work was supported by the National Natural Science Foundation of China (21375043).

## Notes and references

- H. Zhang, M. Jin, Y. Xiong, B. Lim and Y. Xia, *Acc. Chem. Res.*, 2013, **46**, 1783–1794.
- L. Zhang, Z. Xie and J. Gong, *Chem. Soc. Rev.*, 2016, **45**, 3916–3934.
- Y. Zhou, D. Wang and Y. Li, *Chem. Commun.*, 2014, **50**, 6141–6144.
- F. Jiang, R. Li, J. Cai, W. Xu, A. Cao, D. Chen, X. Zhang, C. Wang and C. Shu, *J. Mater. Chem. A*, 2015, **3**, 19433–19438.
- W. Hong, C. Shang, J. Wang and E. Wang, *Energy Environ. Sci.*, 2015, **8**, 2910–2915.
- C. Xu, Q. Hao and H. Duan, *J. Mater. Chem. A*, 2014, **2**, 8875–8880.
- J. Wei, X. Chen, S. Shi, S. Mo and N. Zheng, *Nanoscale*, 2015, **7**, 19018–19026.
- H. Wu, H. Li, Y. Zhai, X. Xu and Y. Jin, *Adv. Mater.*, 2012, **24**, 1594–1597.
- K. Cai, Y. Liao, H. Zhang, J. Liu, Z. Lu, Z. Huang, S. Chen and H. Han, *ACS Appl. Mater. Interfaces*, 2016, **8**, 12792–12797.
- W. Hong, J. Wang and E. Wang, *ACS Appl. Mater. Interfaces*, 2014, **6**, 9481–9487.
- Y.-Y. Feng, Z.-H. Liu, Y. Xu, P. Wang, W.-H. Wang and D.-S. Kong, *J. Power Sources*, 2013, **232**, 99–105.
- J. Huang, Y. Zhu, M. Lin, Q. Wang, L. Zhao, Y. Yang, K. X. Yao and Y. Han, *J. Am. Chem. Soc.*, 2013, **135**, 8552–8561.
- H. Zhang, T. Watanabe, M. Okumura, M. Haruta and N. Toshima, *Nat. Mater.*, 2012, **11**, 49–52.
- L. Carbone and P. D. Cozzoli, *Nano Today*, 2010, **5**, 449–493.
- Y. Liu, G. Zhao, D. Wang and Y. Li, *Natl. Sci. Rev.*, 2015, **2**, 150–166.
- P. S. Lutz, I.-T. Bae and M. M. Maye, *Nanoscale*, 2015, **7**, 15748–15756.
- Y. Sun, *Natl. Sci. Rev.*, 2015, **2**, 329–348.
- S. Cao, F. Tan, Y. Tang, Y. Li and J. Yu, *Chem. Soc. Rev.*, 2016, **45**, 4747–4765.
- X. Liu, D. Wang and Y. Li, *Nano Today*, 2012, **7**, 448–466.
- S. Mourdikoudis, M. Chirea, D. Zanaga, T. Altantzis, M. Mitrakas, S. Bals, L. M. Liz-Marzán, J. Pérez-Juste and I. Pastoriza-Santos, *Nanoscale*, 2015, **7**, 8739–8747.
- W.-Y. Yu, G. M. Mullen, D. W. Flaherty and C. B. Mullins, *J. Am. Chem. Soc.*, 2014, **136**, 11070–11078.
- C.-H. Cui, J.-W. Yu, H.-H. Li, M.-R. Gao, H.-W. Liang and S.-H. Yu, *ACS Nano*, 2011, **5**, 4211–4218.
- B. Lim, H. Kobayashi, T. Yu, J. Wang, M. J. Kim, Z.-Y. Li, M. Rycenga and Y. Xia, *J. Am. Chem. Soc.*, 2010, **132**, 2506–2507.
- B. Wu and N. Zheng, *Nano Today*, 2013, **8**, 168–197.
- J. Zhu, J. Wu, F. Liu, R. Xing, C. Zhang, C. Yang, H. Yin and Y. Hou, *Nanoscale*, 2013, **5**, 9141–9149.
- Q. Cai, S. Lu, F. Liao, Y. Li, S. Ma and M. Shao, *Nanoscale*, 2014, **6**, 8117–8123.
- A. Villa, N. Dimitratos, C. E. Chan-Thaw, C. Hammond, G. M. Veith, D. Wang, M. Manzoli, L. Prati and G. J. Hutchings, *Chem. Soc. Rev.*, 2016, **45**, 4953–4994.
- J. Wu, Y. Hou and S. Gao, *Nano Res.*, 2011, **4**, 836–848.

- 29 Q. Zhang, X. Guo, Z. Liang, J. Zeng, J. Yang and S. Liao, *Nano Res.*, 2013, **6**, 571–580.
- 30 A. Wang, X. Y. Liu, C.-Y. Mou and T. Zhang, *J. Catal.*, 2013, **308**, 258–271.
- 31 K. Cai, X. Xiao, H. Zhang, Z. Lu, J. Liu, Q. Li, C. Liu, M. F. Foda and H. Han, *Nanoscale*, 2015, **7**, 18878–18882.
- 32 H.-W. Liang, S. Liu, J.-Y. Gong, S.-B. Wang, L. Wang and S.-H. Yu, *Adv. Mater.*, 2009, **21**, 1850–1854.
- 33 Y. Wu, D. Wang and Y. Li, *Chem. Soc. Rev.*, 2014, **43**, 2112–2124.
- 34 Z. Dong, X. Le, C. Dong, W. Zhang, X. Li and J. Ma, *Appl. Catal., B*, 2015, **162**, 372–380.